Millimeter Wave-based Fronthaul Network for Cell-free Massive MIMO

Mohamed Ibrahim, Salah Elhoushy, and Walaa Hamouda
Department of Electrical and Computer Engineering, Concordia University,
Montreal, Quebec, Canada
Email: {mo_halil, s_elhosh, hamouda}@encs.concordia.ca

ICC 2022 - IEEE International Conference on Communications | 978-1-5386-8347-7/22/$31.00 ©2022 IEEE | DOI: 10.1109/ICC45855.2022.9838417

***Abstract*—One of the major technological breakthroughs to support unprecedented demands of the future generations of wireless communication networks is cell-free (CF) massive multiple-input multiple-output (mMIMO). However, a fronthaul network with high and reliable capacity links is a prerequisite to realize the full potential of the CF mMIMO. Aiming at deploying a cost-efficient fronthaul network, this paper proposes a millimeter wave (mmWave)-based fronthaul network for the CF mMIMO system operation thanks to the broad bandwidth in the mmWave frequency band. Stochastic geometry tools have been exploited to reflect the impact of the considered fronthaul network on the uplink (UL) performance of CF mMIMO systems. Results reveal that increasing the blockage density deteriorates the average UL data rates, however, increasing the density of CPUs can limit the blockages effect on the system performance. Besides, while it is more preferable to deploy a large number of antennas per access points (AP)s under low blockage densities, having a large number of APs, provided with a small number of antennas leads to superior UL data rates at high blockage densities.**

***Index Terms*—Cell-free mMIMO, mmWave, fronthaul network, UL data rates, stochastic geometry.**

I. Introduction

Many widely anticipated future services including smart manufacturing, telehealth, intelligent transportation, smart homes, and augmented/virtual reality applications will lay the foundation of a more connected society. The essential requirements for future wireless communication networks (5G and beyond) to support such services are to have the ability to provide a broad range of application domains [1]. More specifically, it is projected that mobile traffic will grow in the coming years in the order of thousands compared to current demand. To satisfy such requirements, cell-free (CF) massive multiple-input multiple-output (mMIMO) systems are proposed for 5G and beyond networks operation [2]. In CF mMIMO systems, all access point (AP)s are distributed in the coverage area connected to a central processing unit (CPU) which operates all APs as a mMIMO network with no cell boundaries to jointly serve all users on the same time-frequency resources by means of spatial multiplexing [3], [4]. The performance of CF mMIMO in-terms of the downlink (DL) and uplink (UL) achievable data rates is compared with that of small-cell (SC) systems [5]–[7]. The obtained results revealed that the CF massive mMIMO system provides better performance in terms of the $95\%-$likely per-user throughput.

The capacity of fronthaul networks strongly affects the performance of the CF mMIMO systems. The reason is that the fronthaul networks are responsible for exchanging the data between CPU and the APs. Thus, as the amount of the transferred data in the fronthaul network gets higher, this urges the need for higher fronthaul capacity. Hence, the works in [8]–[10] have investigated the impact of limited capacity of fronthaul networks on the UL performance of CF mMIMO systems. The UL transmission schemes between CPU and AP in the literature can be one of three approaches. The first approach is a Estimate-Compress-Forward (ECF) in which APs will locally estimate the channels for the users, and then the user's data as well as estimated channels are compressed and transmitted to the CPU to perform the detection process. The second one is a Compress-Forward-Estimate (CFE) in which APs compress and transmit the estimated channels and users' data to CPU, and the CPU is responsible for both channel estimation and users' data detection processes. The last approach is a Estimate-Detect-Compress-Forward (EDCF) approach in which the APs locally perform both channel estimation and data detection. Then, APs compress and transmit the local detected data to the CPU.

Considering the UL data rate maximization of limited fronthaul CF mMIMO under maximum ratio combining (MRC) detection, the authors in [8] proposed a low-complexity fronthaul rate allocations with capacity allocation among pilot and data transmission. Results revealed that the achievable data rates are significantly improved for EDCF. Also, the fronthaul capacity for the pilot transmission should be optimized to maximize the achievable UL data rates for ECF and CFE. The authors in [9], [10] investigated the max-min fairness problem of limited fronthaul capacity under EDCF. In this regard, the authors decoupled this non-convex problem into two problems, namely, receiver filter design and power allocation where the optimal solution is achieved by solving these problems iteratively. Results revealed that the achievable UL data rates are significantly improved by applying the two-stage UL data detection while optimizing the receiver filter coefficients.

The fronthaul network of CF mMIMO systems can be deployed either wired or wireless technology. Despite deploying a wired fronthaul solution can provide enormous capacity links, especially using optical fiber, this will significantly increase the construction cost due to the massive number of links to be established between CPU and APs. On the other hand,

the wireless fronthaul network reduces the implementation cost and installation time, and enhances the flexibility and scalability of the network deployment. However, the major challenge with the wireless solution is to support high reliable links with high-capacity for the fronthaul network. Particularly, using the microwave band may lead to a degradation in the performance of CF mMIMO systems due to the limited available bandwidth. Motivated by the broad bandwidth as well as high beamforming gain of the millimeter wave (mmWave) bands, a mmWave fronthaul network may play an essential role in data exchange between the CPU and APs [11]–[13]. For instance, one can operate the fronthaul network at 73 GHz where the available contiguous bandwidth is up to 5 GHz [2]. In that, such high bandwidth can deal with the enormous amount of data transfer in the fronthaul network of CF mMIMO systems.

In this paper, we analyze the effect of deploying a mmWave fronthaul network on the performance of CF mMIMO systems in-terms of achievable UL data rates. Particularly, we consider that the network consists of multiple CPUs to which APs are associated in a distance-based association criterion. The main potential contribution of the paper is three-fold. We firstly exploit stochastic geometry tools to derive the density of active APs, which hold line-of-sight (LoS) fronthaul link with the associated CPU, as a function of densities for both blockages and CPUs. Secondly, we provide an analytical framework to derive the average UL data rates as a function of the active APs density considering the system operation under the EDCF transmission approach. Thirdly, capitalizing on the proposed framework, we give a comprehensive study of the impacts of system parameters on the average UL data rates under mmWave fronthaul network.

The organization of the rest paper is as follows. In Section II, we present the system model. The active APs density , UL channel estimation, and UL performance analysis are discussed in Section III. Simulation studies and discussions are presented in Section IV. Finally, Section V concludes the paper.

II. System Model

We consider a CF mMIMO system consisting of multiple CPUs. We assume that the signal processing tasks are distributed among different physical CPUs which are connected together and spatially distributed according to a homogeneous Poisson Point Process (PPP) with density λ_c. Also, APs and users are distributed according to a homogeneous PPP with densities λ_a and λ_u, respectively. All APs are equipped with N_{ap} antennas, whereas user equipments (UEs) are assumed to be single-antenna terminals. We consider that APs are divided into disjointed sets where the APs in each set are associated to the nearest CPU. We also consider the presence of static blockages (buildings) as shown in Fig. 1. In particular, the centers of blockages are modeled as PPP with density λ_b, and each blockage is formed as a rectangle shape. Their lengths and widths are assumed to be independent uniformly distributed over the intervals $[L_{min}, L_{max}]$ and $[W_{min}, W_{max}]$,

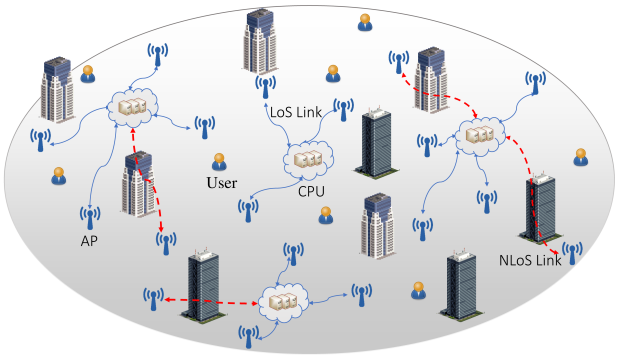

Fig. 1: CF mMIMO system with mmWave fronthaul.

respectively.

A mmWave fronthaul network represent a promising solution to provide the high capacity requirements of CF mMIMO systems due to broad bandwidth and the high beamforming gains in such band. Nevertheless, the short wavelength of mmWave communications poses a critical challenge to the link stability, especially under non LoS communications when the links between the CPU and APs are exposed to random blockages, which in turn may lead to transmission breakdown [14]. As such, a prerequisite for a reliable operation of the mmWave fronthaul network in such band is to have LoS links between the CPUs and their associated APs. Since CPUs and APs are deployed in fixed locations, the buildings are considered as the main obstacle towards having LoS links between the CPUs and their associated APs. In that, the probability of having a LoS mmWave fronthaul link for a certain AP depends on its distance with the associated CPU as well as the density of blockages. The probability of having a LoS fronthaul link with distance r is given by [15]

$$p_{LoS} = e^{-\mathcal{B}r}, \tag{1}$$

with

$$\mathcal{B} = \frac{2\lambda_b(\mathbb{E}[L] + \mathbb{E}[W])}{\pi}, \tag{2}$$

where $\mathcal{B}$ is the blockage density on the link, and $\mathbb{E}[\cdot]$ denotes statistical expectation.

Contrary to the fronthaul transmission, the environment around users includes static and mobile objects that may totally block the LoS links between APs and users. In addition, the mobility of users may make wireless channels with APs switch between blocked and unblocked conditions. Hence, we consider the microwave band for access links due to its high reliability. We model the channels between APs and users as Rayleigh fading channels. As such, the channel vector between the m^{th} AP and the k^{th} user $\boldsymbol{g}_{mk} \in \mathbb{C}^{N_{ap}\times 1}$ is expressed as

$$\boldsymbol{g}_{mk} = \sqrt{\beta_{mk}}\boldsymbol{h}_{mk}, \tag{3}$$

with

$$\beta_{mk} = d_{mk}^{-3.5}\ \mathbf{1}(d_{mk} > 50) + 50^{-1.5} d_{mk}^{-2}\ \mathbf{1}(10 \le d_{mk} \le 50) + 50^{-1.5}10^{-2}\ \mathbf{1}(d_{mk} < 10), \tag{4}$$

where β_{mk} represents the large-scale fading coefficient which is calculated using the three-slope path-loss models [16], $\mathbf{1}(\cdot)$ is the indicator function, and d_{mk} represents the distance between the m^{th} AP and the k^{th} user. Furthermore, $\boldsymbol{h}_{mk} \in \mathbb{C}^{N_{ap}\times 1}$ is a vector of the small-scale fading coefficients whose entries are independent and identically distributed (i.i.d.) $\mathcal{CN}(0,1)$.

III. Performance Evaluation

In this section, we investigate the UL performance of CF mMIMO in the presence of mmWave fronthaul network. Firstly, stochastic geometry is applied in order to derive the density of active APs (APs with LoS fronthaul links with their associated CPUs). Then, we derive the average achievable UL data rates of CF mMIMO systems.

A. Active APs Density

Some APs may not be competent to exchange user's data with their associated CPUs. This is because their fronthaul link with their CPU are exposed to blockages. Hence, we investigate the impact of the blockages on the density of activated APs which have LoS link with its associated CPUs. Note that, the activation of a particular AP depends mainly on the density of blockage and its distance with its associated CPU. As such, the activated APs can be released as being generated from an independent thinning operation over the entire existing APs PPP [17]. In that, the corresponding density of activated APs will be $\widetilde{\lambda}_a = p_a \times \lambda_a$, where p_a is the probability of AP activation. We consider that APs are associated with the nearest CPU where the distance distribution between the AP and the nearest CPU is given by

$$f_R(r) = 2\pi\lambda_c\ re^{-\pi\lambda_c r^2}. \tag{5}$$

Using the distance distribution, we evaluate the activation probability p_a as follows:

$$\begin{aligned} p_a = P(N_B(AP,CPU)=0) &= \int_0^\infty e^{-\mathcal{B}r} 2\pi\lambda_c\ re^{-\pi\lambda_c r^2}\ dr, \\ &= 1-\mathcal{B}\int_0^\infty e^{-\mathcal{B}r}e^{-\pi\lambda_c r^2}\ dr = 1-\frac{\mathcal{B}e^{\frac{\mathcal{B}^2}{4\pi\lambda_c}}}{2\sqrt{\lambda_c}} erfc\Big[\frac{\mathcal{B}}{2\sqrt{\pi\lambda_c}}\Big], \end{aligned} \tag{6}$$

where $N_B(AP,CPU)$ denotes the number of blockages on the link between the AP and CPU, and erfc is the complementary error function.

B. Uplink Channel Estimation

Time-division duplexing (TDD) is considered for system operation. Thus, in the first transmission phase, all users send training sequences so that APs can estimate their channel conditions. In that, for ease of analysis and tractability, we assume that users are assigned mutually-orthogonal pilot sequences of length $\tau_p \geq K$ symbols. Let us assume that $\boldsymbol{\psi}_k \in \mathbb{C}^{\tau_p\times 1}$ denotes the assigned pilot sequence to user k, the received pilot sequence at the *m*-th active AP is given by

$$\boldsymbol{Y}_{p,m} = \sqrt{P_p\tau_p}\sum_{k=1}^{K}\boldsymbol{g}_{mk}\boldsymbol{\psi}_k^T + \boldsymbol{W}_{p,m}, \tag{7}$$

where P_p denotes the UL transmit power of each pilot symbol, and $\boldsymbol{W}_{p,m} \in \mathbb{C}^{N_{ap}\times\tau_p}$, the matrix at the m-th active AP whose vectors follow $\mathcal{CN}(\mathbf{0},\sigma_w^2\boldsymbol{I}_{N_{ap}})$. Each active AP, *m*, computes the minimum mean-square error (MMSE) estimate of the channel coefficient $g_{mk}, \forall k$. In that, the estimated channel $\hat{\boldsymbol{g}}_{mk}$ and the channel estimation error $\tilde{\boldsymbol{g}}_{mk}$ are modeled by

$$\hat{\boldsymbol{g}}_{mk}\ \sim\ \mathcal{CN}(0,\ \eta_{mk}I_{N_{ap}}), \tag{8}$$

$$\tilde{\boldsymbol{g}}_{mk}\ \sim\ \mathcal{CN}(0,\ (\beta_{mk}-\eta_{mk})I_{N_{ap}}), \tag{9}$$

where

$$\eta_{mk} = \frac{P_p\tau_p\beta_{mk}^2}{P_p\tau_p\beta_{mk}+\sigma_w^2}. \tag{10}$$

C. Uplink Performance Analysis

In what follows, we provide an analytical framework to derive the average UL data rates of CF mMIMO as a function of the density of activated APs. In that, we apply local MRC for UL data detection during the UL transmission phase. Without loss of generality, we develop the analysis considering a typical user, located at the origin.

During the UL data transmission phase, each user transmits its UL data symbol to all deployed APs over the whole available time-frequency resources. Then, APs exploit the users' estimated channels to detect the UL transmitted symbol of each user. Assuming equal power allocation and MRC detection, the locally detected UL signal of user o at the $\mathrm{m^{th}}$ AP is given by

$$y_o = \sqrt{P_u}\sum_{k=1}^{K}\hat{\boldsymbol{g}}_{mo}^H\boldsymbol{g}_{mk}s_k + \hat{\boldsymbol{g}}_{mo}^H\boldsymbol{w}_u, \tag{11}$$

where $s_k \sim \mathcal{CN}(0,1)$ is the transmitted UL signal from user k while P_u is the UL transmission power. Also, $\boldsymbol{w}_m \in \mathbb{C}^{1\times N_{ap}}$ is the additive noise vector at the m-th AP whose entries are i.i.d. $\sim\mathcal{CN}(0,1)$. The achievable UL data rate for user o can be calculated using the use-and-then-forget technique [18] as follows:

$$R_o = log_2(1+\gamma_o), \tag{12}$$

with

$$\gamma_o = \frac{P_u\Big(\sum\limits_{m=1}^{M}N_{ap}\ \eta_{mo}\Big)^2}{P_u\sum\limits_{m=1}^{M}N_{ap}\ \eta_{mo}\sum\limits_{k=1}^{K}\beta_{mk}+\sigma_w^2\sum\limits_{m=1}^{M}N_{ap}\ \eta_{mo}\ \beta_{mo}}. \tag{13}$$

Consequently, the average achievable UL data rate over different realizations is given by

$$\bar{R}_o = \mathbb{E}\big[log_2(1+\gamma_o)\big]. \tag{14}$$

One can note that calculating $\bar{R}_o$ is a challenging task since it requires averaging over all users and APs locations. To

circumvent this issue, we need to simplify the expression for γ_o in (13). In doing so and since η_{mo}, β_{mo}, and β_{mk} are monotonically decreasing with distance, we apply the mean plus nearest approximation [19] to simplify each individual term in (13). Accordingly, the term $\sum_{m=1}^{M} \eta_{mo}$ in the numerator can be approximated by

$$\begin{aligned}\sum_{m=1}^{M} \eta_{mo} &\approx \eta(r_1) + \mathbb{E}\Big[\sum_{m'=2}^{M} \eta_{m'o}\big|r_1\Big], \\ &\approx \eta(r_1) + \sum_{m'=2}^{M} \int_{r_1}^{\infty} \eta(r)\ f_{R_{m'}}\big(r\big|r_1\big) dr,\end{aligned} \tag{15}$$

where m' represents the order of the active APs according to their distances with the typical user. Also, the first term represents the nearest AP contribution as a function of its distance with the typical user r_1. The second term reflects the average contribution of other APs, starting from the second nearest AP to the m^{th} nearest AP, conditioned on the user's distance with the first nearest AP r_1. The distance distribution of the m'-th nearest AP given the distance r_1 can be expressed by [20]

$$f_{R_{m'}}\big(r\big|r_1\big) = 2\pi\widetilde{\lambda}_a\ r\ \frac{\big[\pi\widetilde{\lambda}_a(r^2 - r_1^2)\big]^{m'-2}}{(m'-2)!} e^{-\pi\widetilde{\lambda}_a(r^2-r_1^2)}, \tag{16}$$

Thus, (15) can be calculated by

$$\begin{aligned}\sum_{m=1}^{M} \eta_{mo} &= \eta(r_1) + \sum_{m'=2}^{M} \int_{r_1}^{\infty} \eta(r)\ 2\pi\widetilde{\lambda}_a\ r \frac{\big[\pi\widetilde{\lambda}_a(r^2 - r_1^2)\big]^{m'-2}}{(m'-2)!} \\ &\qquad \times e^{-\pi\widetilde{\lambda}_a(r^2-r_1^2)} dr, \\ &= \eta(r_1) + \int_{r_1}^{\infty} \eta(r)\ 2\pi\widetilde{\lambda}_a\ r\ e^{-\pi\widetilde{\lambda}_a(r^2-r_1^2)} \\ &\qquad \times \sum_{m'=2}^{M} \frac{\big[\pi\widetilde{\lambda}_a(r^2 - r_1^2)\big]^{m'-2}}{(m'-2)!} dr,\end{aligned} \tag{17}$$

where

$$\begin{aligned}\sum_{k'=2}^{K} \frac{\big[\pi\widetilde{\lambda}_a(r^2 - r_1^2)\big]^{k'-2}}{(k'-2)!} &= \sum_{k'=0}^{K-2} \frac{\big[\pi\widetilde{\lambda}_a(r^2 - r_1^2)\big]^{k'}}{k'!}, \\ &\overset{(a)}{=}\ e^{\pi\widetilde{\lambda}_a(r^2-r_1^2)} \frac{\Gamma(K-1, \pi\widetilde{\lambda}_a(r^2 - r_1^2))}{\Gamma(K-1)}, \\ &\overset{(b)}{\approx}\ e^{\pi\widetilde{\lambda}_a(r^2-r_1^2)},\end{aligned} \tag{18}$$

with $\Gamma(\cdot\ ,\ \cdot)$ denotes the lower incomplete gamma function. Then, to simplify $\overset{(a)}{=}$, we consider an asymptotic approach assuming $K \to \infty$ which results in a simpler form as shown in $\overset{(b)}{\approx}$. Hence, the numerator in (13) can be approximated by

$$\sum_{m=1}^{M} \eta_{mo} \approx \eta(r_1) + \int_{r_1}^{\infty} \eta(r)\ 2\pi\widetilde{\lambda}_a r\ dr. \tag{19}$$

Regarding the denominator in (13), we firstly neglect the effect of the noise. Then, applying some mathematical manipulations, the denominator can be expressed by

$$\begin{aligned}\sum_{m=1}^{M} \eta_{mo} \sum_{k=1}^{K} \beta_{mk} &= \sum_{m=1}^{M} \eta_{mo}\beta_{mo} + \sum_{m=1}^{M} \eta_{mo} \sum_{k\neq o}^{K} \beta_{mk}, \\ &\approx\ \eta(r_1)\ \beta(r_1) + \mathbb{E}\Big[\sum_{m'=2}^{M} \eta_{m'o}\beta_{m'o}\big|r_1\Big] + \sum_{m=1}^{M} \eta_{mo} \sum_{k\neq o}^{K} \beta_{mk},\end{aligned} \tag{20}$$

Then, following the same procedure as (17) and (18), the second term in (20) can be calculated by

$$\begin{aligned}\mathbb{E}\Big[\sum_{m'=2}^{M} \eta_{m'o}\beta_{m'o}\big|r_1\Big] &= \sum_{m'=2}^{M} \int_{r_1}^{\infty} \eta(r)\ \beta(r)\ f_{R_{m'}}\big(r\big|r_1\big)\ dr, \\ &= \int_{r_1}^{\infty} \eta(r)\ \beta(r)\ 2\pi\widetilde{\lambda}_a\ r\ dr.\end{aligned} \tag{21}$$

Also, the third term in (20) can be approximated by

$$\begin{aligned}\sum_{m=1}^{M} \eta_{mo} \sum_{k\neq o}^{K} \beta_{mk} &\overset{(a)}{\approx}\ \mathbb{E}\Big[\sum_{k\neq o}^{K} \beta_{mk}\Big] \sum_{m=1}^{M} \eta_{mo}, \\ &\approx \int_{0}^{\infty} \beta(r)\ 2\pi\lambda_u r\ dr \times \Big(\eta(r_1) + \mathbb{E}\Big[\sum_{m'=2}^{M} \eta_{m'o}\big|r_1\Big]\Big). \\ &\approx \int_{0}^{\infty} \beta(r)\ 2\pi\lambda_u r\ dr \times \Big(\eta(r_1) + \int_{r_1}^{\infty} \eta(r)\ 2\pi\widetilde{\lambda}_a r\ dr\Big)\end{aligned} \tag{22}$$

where in $\overset{(a)}{\approx}$, we assume that the summation of large-scale fading coefficients of users on each active AP is independent of the AP index to simplify the calculation of this term. Then, the mean plus nearest approximation is applied on the summation over the channel estimation variances of the typical user. By substituting (21) and (22) in (20) followed by applying (19) and (20) in (13), one can note that γ_o in (13) becomes only a function of the distance of the nearest AP to the typical user r_1. As such, the average UL data rate in (14) can be calculated by averaging only over the distance r_1 as follows:

$$R_o = \int_{0}^{\infty} log_2\big(1 + \gamma_o\big) \times 2\pi\widetilde{\lambda}_a r_1 e^{-\pi\widetilde{\lambda}_a r_1^2}\ dr_1. \tag{23}$$

IV. Simulation Results

The simulation parameters are given as follows. Firstly, the CPUs, APs and users are uniformly distributed in a cell with radius $\mathcal{R} = 500$ m. Results are generated assuming a carrier frequency for the access links $f_c = 2$ GHz. Also, the UL pilot and data transmission powers are equal with $P_p = P_u = 100$ mW [16]. The noise variance $\sigma_w^2 = 290{\times}\kappa{\times}B_a{\times}NF$ where κ is the Boltzman constant, $B_a = 20$ MHz, denoting the system

bandwidth of access links, and $NF = 9$ dB is the noise figure [21]. We also consider the length and width parameters of blockages are [10 m, 25 m], and [10 m, 20 m], respectively [22]. Also, all APs are equipped with $N_{ap} = 4$ antennas, and the densities of APs, users, and CPUs are $\lambda_a = 500/km^2$, $\lambda_u = 75/km^2$, and $\lambda_c = 6/km^2$, respectively, unless otherwise specified.

Fig. 2 depicts the average UL data rates at different densities of blockages and CPUs. As noted, the analytical results in (23) are consistent with simulations at different system settings. It is clear that the average UL data rates decrease as the density of blockages gets higher. This is a consequence of the smaller number of activated APs at higher densities of blockages. However, increasing the number of CPUs remarkably improves the average UL data rates as a result of limiting the number of deactivated APs due to blockages. Besides, the increase in the average UL data rates declines as the density of CPUs gets higher since a reasonable number of APs has been already activated.

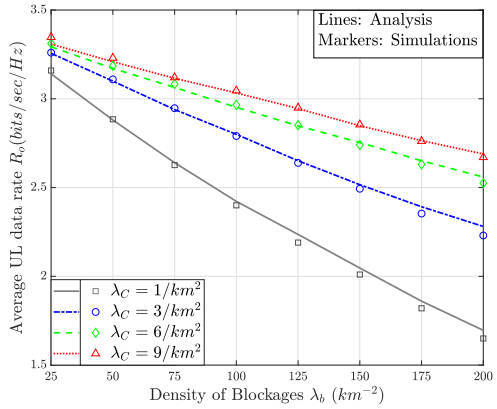

Fig. 2: Average uplink data rates at different densities of blockages and CPUs.

Considering different target APs activation probabilities, Fig. 3 depicts the required density of CPUs to achieve such APs activation probabilities under different blockage densities. It is noted that the required density of CPUs significantly increases with the density of blockages. This can be interpreted from (6) where doubling the blockage density increases the required density of CPUs by four-fold to maintain the same activation probability. Also, it can be noted from (6) that, at a certain blockage density, the activation probability is a logarithmically increasing function of λ_c. Hence, the required CPUs density exponentially increases with the activation probability. This reflects the significant increase in the required CPUs density as the activation probability increases from $p_a = 0.8$ to $p_a = 0.9$ under different blockage densities. This in turn leads to an extremely high density of required CPUs at higher blockage densities. However, since such high number of CPUs is practically not feasible, it is required to evaluate the performance loss at low activation probabilities compared to higher ones.

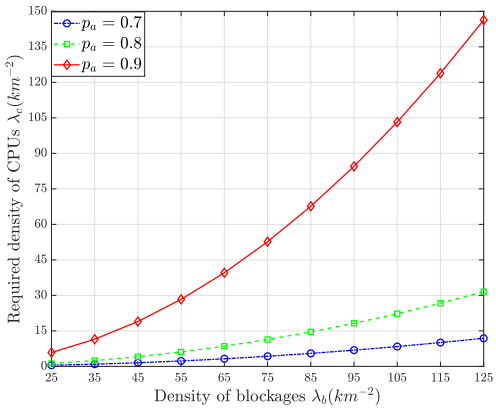

Fig. 3: Required density of CPUs for certain APs activation probability under different densities of blockages.

Fig. 4 shows the introduced loss on the average UL data rates under different APs activation probabilities. The loss is calculated relative to the ideal case where all APs are activated. Intuitively, the introduced loss in the average UL data rates reduces with increasing the activation probability. Also, for the same APs activation probability, having larger densities of APs can limit the introduced loss in the UL data rates. In addition, to keep the performance loss below a certain level, systems with higher densities of APs require lower APs activation probabilities, compared to systems with lower densities of APs. This in turn limits the required density of CPUs for the system operation, especially under high blockage scenarios as shown in Fig. 3.

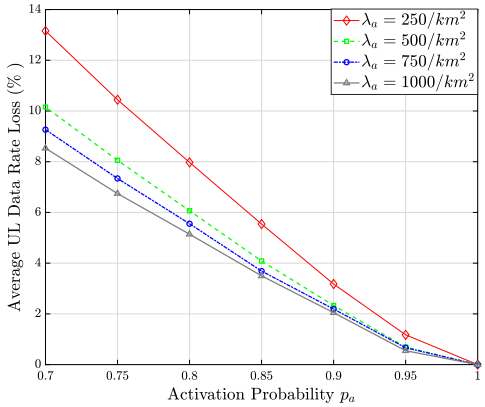

Fig. 4: Average uplink data rates loss due to certain activation probability for different densities of APs.

In Fig. 5, the average UL data rates are shown at different blockage densities under different network configurations. In particular, we consider different combinations of AP densities and number of antennas per APs in each configuration. Also, for a fair comparison, we consider that the total number of antennas in the system is the same for different configurations. Note that, CF mMIMO systems suffer from a lack of channel hardening since each user receives different

channel gains from the spatially distributed APs [23]. Also, such lack of channel hardening significantly deteriorates the system performance. However, one way to reduce this effect is through increasing the number of antennas at each AP. As such, one can observe that under low blockage densities ($\lambda_b = 25 - 75/km^2$), increasing the number of antennas per AP ($\lambda_a = 100/km^2,\ N_{ap} = 20$) attains superior average UL data rates. However, this does not hold at higher blockage densities where it turns out that improving the provided spatial diversity gains through deploying a larger number of APs with small number of antennas is more beneficial for the system performance. This can be reflected by the superiority of $\lambda_a = 500/km^2,\ N_{ap} = 4$ in achieving higher UL data rates compared to $\lambda_a = 100/km^2,\ N_{ap} = 20$ when $\lambda_b > 85/km^2$.

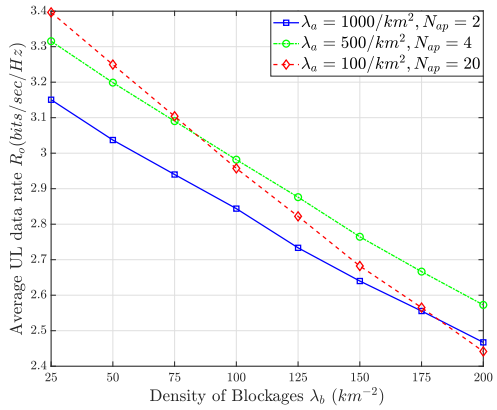

Fig. 5: Average uplink data rates versus density of blockages for different numbers of antennas at AP and densities of APs.

V. Conclusion

We investigated the impact of mmWave fronthaul network on the UL performance of CF mMIMO systems. We assumed that the system consists of multiple CPUs to which APs are associated in a distance-based association approach. Based on this and using tools from stochastic geometry, we derived the density of activated APs as a function of the blockage and CPU densities. Then, we obtained the average UL data rates as a function of the density of active APs. We showed that the UL data rates are significantly affected by the density of blockages in the network. However, increasing the density of CPUs can alleviate the performance degradation at high blockage densities. Besides, the network deployment should be adjusted according to the blockage densities. In particular, deploying a large number of APs, equipped with a small number of antennas leads to superior UL data rates at high blockage densities. However, a larger number of antennas per APs attains higher UL performance under low blockage densities.

References

[1] M. Matthaiou, O. Yurduseven, H. Q. Ngo, D. Morales-Jimenez, S. L. Cotton, and V. F. Fusco, "The Road to 6G: Ten Physical Layer Challenges for Communications Engineers," *IEEE Communications Magazine*, vol. 59, no. 1, pp. 64–69, 2021.

[2] S. Elhoushy, M. Ibrahim, and W. Hamouda, "Cell-Free Massive MIMO : A Survey," *IEEE Communications Surveys & Tutorials*, pp. 1–1, 2021, (to appear).

[3] A. Papazafeiropoulos, P. Kourtessis, M. D. Renzo, S. Chatzinotas, and J. M. Senior, "Performance analysis of cell-free massive MIMO systems: A stochastic geometry approach," *IEEE Transactions on Vehicular Technology*, vol. 69, no. 4, pp. 3523–3537, 2020.

[4] A. Adhikary, J. Nam, J. Ahn, and G. Caire, "Joint spatial division and multiplexing–the large-scale array regime," *IEEE Transactions on Information Theory*, vol. 59, no. 10, pp. 6441–6463, Oct 2013.

[5] E. Nayebi, A. Ashikhmin, T. L. Marzetta, H. Yang, and B. D. Rao, "Precoding and power optimization in cell-free massive MIMO systems," *IEEE Transactions on Wireless Communications*, vol. 16, no. 7, pp. 4445–4459, 2017.

[6] E. Björnson and L. Sanguinetti, "Making cell-free massive MIMO competitive with MMSE processing and centralized implementation," *IEEE Transactions on Wireless Communications*, vol. 19, no. 1, pp. 77–90, 2020.

[7] S. Elhoushy and W. Hamouda, "Towards high data rates in dynamic environments using hybrid cell-free massive MIMO/small-cell system," *IEEE Wireless Communications Letters*, pp. 1–1, 2020.

[8] H. Masoumi and M. J. Emadi, "Performance analysis of cell-free massive MIMO system with limited fronthaul capacity and hardware impairments," *IEEE Transactions on Wireless Communications*, vol. 19, no. 2, pp. 1038–1053, 2020.

[9] M. Bashar, K. Cumanan, A. G. Burr, H. Q. Ngo, and M. Debbah, "Cell-free massive MIMO with limited backhaul," in *2018 IEEE International Conference on Communications (ICC)*, 2018, pp. 1–7.

[10] M. Bashar *et al.*, "Max–Min rate of cell-free massive MIMO uplink with optimal uniform quantization," *IEEE Transactions on Communications*, vol. 67, no. 10, pp. 6796–6815, 2019.

[11] M. Ibrahim and W. Hamouda, "Reliable Millimeter Wave Communication for IoT Devices," in *ICC 2021 - IEEE International Conference on Communications*, 2021, pp. 1–6.

[12] R. G. Stephen and R. Zhang, "Joint millimeter-wave fronthaul and OFDMA resource allocation in ultra-dense CRAN," *IEEE Transactions on Communications*, vol. 65, no. 3, pp. 1411–1423, 2017.

[13] X. Wang *et al.*, "Millimeter wave communication: A comprehensive survey," *IEEE Communications Surveys & Tutorials*, vol. 20, no. 3, pp. 1616–1653, 2018.

[14] M. Ibrahim and W. Hamouda, "Performance analysis of minimum hop count-based routing techniques in millimeter wave networks: A stochastic geometry approach," *IEEE Transactions on Communications*, vol. 69, no. 12, pp. 8304–8318, 2021.

[15] M. Ibrahim, W. Hamouda, and S. Muhaidat, "Spectral efficiency of multi-hop millimeter wave networks using N^{th} best relay routing technique," *IEEE Transactions on Vehicular Technology*, vol. 69, no. 9, pp. 9951–9959, 2020.

[16] S. Elhoushy and W. Hamouda, "Limiting doppler shift effect on cell-free massive MIMO systems: A stochastic geometry approach," *IEEE Transactions on Wireless Communications*, pp. 1–1, 2021.

[17] M. Haenggi, "Stochastic geometry for wireless networks, cambridge uni," 2013.

[18] S. Elhoushy and W. Hamouda, "Performance of distributed massive MIMO and small-cell systems under hardware and channel impairments," *IEEE Transactions on Vehicular Technology*, vol. 69, no. 8, pp. 8627–8642, 2020.

[19] P. Parida, H. S. Dhillon, and A. F. Molisch, "Downlink performance analysis of cell-free massive MIMO with finite fronthaul capacity," in *2018 IEEE 88th Vehicular Technology Conference (VTC-Fall)*, Aug 2018, pp. 1–6.

[20] D. Moltchanov, "Distance distributions in random networks," *Ad Hoc Networks*, vol. 10, no. 6, pp. 1146–1166, 2012.

[21] S. Elhoushy and W. Hamouda, "Downlink performance of limited-fronthaul cell-free massive mimo," in *ICC 2021 - IEEE International Conference on Communications*, 2021, pp. 1–6.

[22] M. Ibrahim and W. Hamouda, "Impact of limited hop count on connectivity of millimeter wave networks," in *GLOBECOM 2020 - 2020 IEEE Global Communications Conference*, 2020, pp. 1–6.

[23] Z. Chen and E. Björnson, "Channel hardening and favorable propagation in cell-free massive MIMO with stochastic geometry," *IEEE Transactions on Communications*, vol. 66, no. 11, pp. 5205–5219, 2018.